ACCOUNTS of chemical research

Article

pubs.acs.org/accounts

Spectroscopic Properties of Doped and Defective Semiconducting Oxides from Hybrid Density Functional Calculations

Cristiana Di Valentin* and Gianfranco Pacchioni*

Dipartimento di Scienza dei Materiali, Università di Milano-Bicocca via R. Cozzi 55 20125 Milano, Italy

CONSPECTUS: Very rarely do researchers use metal oxides in their pure and fully stoichiometric form. In most of the countless applications of these compounds, ranging from catalysis to electronic devices, metal oxides are either doped or defective because the most interesting chemical, electronic, optical, and magnetic properties arise when foreign components or defects are introduced in the lattice. Similarly, many metal oxides are diamagnetic materials and do not show a response to specific spectroscopies such as electron paramagnetic resonance (EPR) spectroscopy. However, doped or defective oxides may exhibit an interesting and informative paramagnetic behavior.

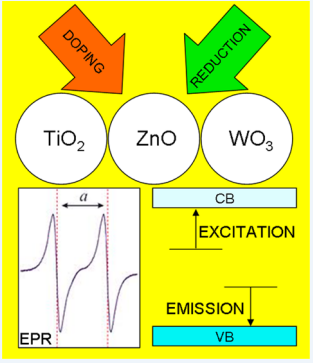

Doped and defective metal oxides offer an expanding range of applications in contemporary condensed matter science; therefore researchers have devoted enormous effort to the understanding their physical and chemical properties. The interplay between experiment and computation is particularly useful in this field, and contemporary simulation techniques have achieved high accuracies with these materials.

In this Account, we show how the direct comparison between spectroscopic experimental and computational data for some selected and relevant materials provides ways to understand and control these complex systems. We focus on the EPR properties and electronic transitions that arise from the presence of dopants and defects in bulk metal oxide materials. We analyze and compare the effect of nitrogen doping in TiO_2 and ZnO (two semiconducting oxides) and MgO (a wide gap insulator) and examine the effect of oxygen deficiency in the semiconducting properties of TiO_{2-x}, ZnO_{1-x}, and WO_{3-x} materials. We chose these systems because of their relevance in applications including photocatalysis, touch screens, electrodes in magnetic random access memories, and smart glasses.

Density functional theory (DFT) provides the general computational framework used to illustrate the electronic structure of these systems. However, for a more accurate description of the oxide band gap and of the electron localization of the impurity states associated with dopants or defects, we resorted to the use of hybrid functionals (B3LYP), where a portion of exact exchange in the exchange-correlation functional partly corrects for the self-interaction error inherent in DFT. In many cases, the self-interaction correction is very important, and these results can lead to a completely different physical picture than that obtained using local or semilocal functionals. We analyzed the electronic transitions in terms of their transition energy levels, which provided a more accurate comparison with experimental spectroscopic data than Kohn−Sham eigenvalues.

The effects of N-doping were similar among the three oxides that we considered. The nature of the impurity state is always localized at the dopant site, which may limit their application in photocatalytic processes. Photocatalytic systems require highly delocalized photoexcited carriers within the material to effectively trigger redox processes at the surface.

The nature of the electronic states associated with the oxygen deficiency differed widely in the three investigated oxides. In ZnO_{1-x} and WO_{3-x} the electronic states resemble the typical F-centers in insulating oxides or halides, with the excess electron density localized at the vacancy site. However, TiO_2 acts as a reducible oxide, and the removal of neutral oxygen atoms reduced Ti^{4+} to Ti^{3+}.

1. INTRODUCTION

Doped and defective semiconducting oxides are topical systems in contemporary material science and attract much interest both because of the fundamental challenges their properties pose and because of the broad range of key technologies in which they are involved. For example, doped TiO_2 is used in visible-light photocatalysis,[1] doped ZnO as a transparent semiconducting oxide[2] for touch screens, displays, or solar cells, and oxygen deficient WO_{3-x} as a component in smart windows for its electrochromic properties.[3] In general, electronic and magnetic properties that appear in the presence of a certain concentration of dopants or defects, often associated to trapping or self-trapping phenomena, are crucial in determining the role played by these types of materials in the various applications.

The controlled introduction of dopants and defects in metal oxides widely expands the range of possible materials with new and more peculiar properties than their parent systems.[4,5] For this reason, they are among the most widely studied materials being the object of continuous and extensive research, both experimental and theoretical. The synergy between the

Special Issue: DFT Elucidation of Materials Properties

Received: December 16, 2013
Published: May 14, 2014

experimental and the computational work is a key aspect in this research field, leading to an effective scientific advancement in the understanding of such complex systems. In this Account, we will present, for a sample of selected cases, existing tools that allow us to directly link experimental spectroscopic results with quantum mechanically computed quantities. In particular, attention will be focused on the investigation of the electron paramagnetic resonance (EPR) properties (section 2) and of the electronic transitions (section 3) of the chosen systems. We will compare three N-doped metal oxides, TiO_2, ZnO, and MgO, and three oxygen deficient semiconducting oxides, TiO_{2-x}, ZnO_{1-x}, and WO_{3-x}, with very different geometrical and electronic structure. While TiO_2, ZnO, and WO_3 are semiconductors with optical band gaps of 3.0−3.4 eV (rutile−anatase),[6,7] 3.44 eV,[8] and 3.1 eV,[9] respectively, MgO is an insulator with a band gap of 7.6−7.8 eV.[10] From this comparison, we will learn how the effect of doping and the nature of the oxygen vacancy defect change with the type of oxide and its structure.

The proper reproduction of the band gap in semiconducting or insulating materials is a necessary prerequisite in order to accurately describe the effect of element doping or deficiency on the electronic structure and properties. It is common practice to estimate the semiconductor band gap and the energy levels introduced in the gap by defect centers using the single-particle Kohn−Sham eigenvalues. This approach, however, is not well justified and can be used only for qualitative comparisons with optical or photoemission data. The problem of the position of defect states in the gap can be partly solved by the calculation of the transition energy levels between different defect charge states. As far as the band gap problem is concerned, local and semilocal DFT or Hartree−Fock (HF) calculations either severely underestimate or overestimate, respectively, the band gap. Several studies in recent years have shown that hybrid exchange-correlation functionals, making use of a combination of exact (as in HF) and DFT exchange terms, represent a more practical, with respect to the accurate but too expensive GW methods, although not ideal solution to reproduce the experimental band gap (note that the % of exact exchange to be introduced is materials dependent).[11] This is the approach followed to study the systems described in this Account. In particular, we used the unscreened B3LYP exchange-correlation functional with 20% exact exchange.[12] Among other hybrid functionals, B3LYP has the advantage of providing a generally acceptable description of the Kohn−Sham band gap and allowing the comparison of a large database of molecular and solid state systems computed at this level. Note, however, that in some cases screened functionals[13] may provide a slightly different description when dealing with shallow versus deep defect states. With the B3LYP functional, as implemented in the CRYSTAL09 code,[14] based on localized atomic orbital basis sets, the computed band gaps of TiO_2 (rutile/anatase), ZnO, WO_3, and MgO are 3.53/3.86, 3.38, 3.13, and 6.90 eV, respectively.

2. EPR PROPERTIES OF NITROGEN DOPED METAL OXIDES

2.1. Paramagnetic Defects: Role of EPR

EPR[15,16] is a key technique for the spectroscopic characterization of very small amounts of paramagnetic centers, being able to detect 10^{10} spins. For a complete characterization of the defect, however, a comparison with other spectroscopies or with computed spin properties is often very useful. Key quantities in EPR spectra are the **g**-tensor and the hyperfine coupling constants (hfcc's), which provide a powerful tool to define the level of spin localization. The hfcc with the ^{14}N nuclides will be used in the following to discuss spin properties of N-doped materials. The hyperfine spin-Hamiltonian, $\mathbf{H}_{hfc} = \mathbf{S}\cdot\mathbf{A}\cdot\mathbf{I}$, is given in terms of the hyperfine matrix **A**, which describes the coupling of the electron with the nuclear spin. The components of **A** can be represented as

$$\mathbf{A} = \begin{bmatrix} A_1 & 0 & 0 \\ 0 & A_2 & 0 \\ 0 & 0 & A_3 \end{bmatrix} = a_{iso}\mathbf{U} + \begin{bmatrix} B_1 & 0 & 0 \\ 0 & B_2 & 0 \\ 0 & 0 & B_3 \end{bmatrix}$$

where **U** is the unit matrix. The isotropic part, a_{iso}, of the coupling constant is related to the spin density at the nucleus (the Fermi contact term).

2.2. N-Doping of TiO_2

Nonmetal doping is considered a promising way to improve the photoabsorption properties of TiO_2.[1,17,18] Among the several elements considered, nitrogen doping has attracted great attention and created strong expectations, only partly fulfilled. The reason is now well understood and can be related to the specific nature of the electronic structure of N-induced centers. N-doped TiO_2 has thus become one of the best studied examples of doped semiconducting oxide. The N−TiO_2 saga was started by a work by Asahi et al.[1] where it was proposed, based on non-spin-polarized local density approximation (LDA) calculations with small supercells, that N-doping induces a rigid shift of the top of the VB to higher energies and hence results in improved photocatalytic activity. Unfortunately, several later studies showed unambiguously that the N 2p impurity states are localized on the N atom and their energy levels lie a few tenths of an electronvolt above the VB.[19,20] While this improves visible-light absorption, it also increases the electron−hole recombination rate, thus resulting in a very low efficiency of the photocatalyst. This general and relevant conclusion shows the importance of a proper characterization of the defects induced by doping in a material. Here we briefly review the case of N-doping of anatase TiO_2.

Two different nitrogen species can form in a bulk oxide, namely, N substitutional to a lattice O ion (N_s) and N interstitial (N_i) (see ref 20 and references therein). The electronic structure, the chemical properties, and the behavior of a doped material depend very critically on the position of the dopant.

While replacing an O for a N atom does not imply major structural modifications, the inclusion of an interstitial dopant can result in various configurations. For the case of N, a real chemical interaction takes place and the N_i atom forms a direct bond with a lattice O with formation of a π radical NO species with −2 formal charge bearing three electrons in a π antibonding orbital, Figure 1. The N−O distance is 1.36 Å (gas-phase NO, 1.15 Å). The energy levels of N_s lie 0.13 eV above the edge of the valence band (VB), while those of N_i are a bit higher (0.64 eV).

Theory predicts both N_i and N_s species to be paramagnetic ($N_i^{\bullet}$ and $N_s^{\bullet}$) and indeed EPR experiments performed on sol−gel prepared samples have shown that N−TiO_2 samples absorbing visible light also contain paramagnetic species located in the bulk and characterized by a relevant spin density on a N p orbital.[20] This species (generally labeled N_b with b = bulk to

dx.doi.org/10.1021/ar4002944 | Acc. Chem. Res. 2014, 47, 3233−3241

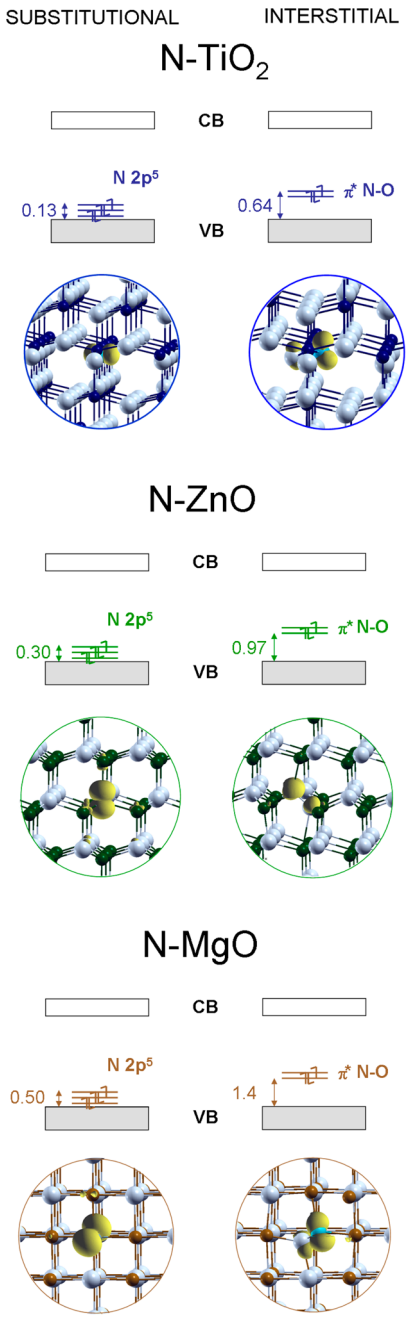

Figure 1. Schematic representation of the Kohn–Sham levels in the band gap of the material (top) and ball-and-stick representation (bottom) with spin density plot (yellow) for substitutional (left) and interstitial (right) nitrogen impurity in anatase TiO_2, wurzite ZnO, and MgO. Ti atoms in blue, Zn atoms in green, Mg atoms in brown, O atoms in gray, and N atoms in light blue.

indicate both N_s and N_i species) changes its intensity under irradiation with visible light and is responsible for photoinduced electron transfer to adsorbates.[20] Thus, N_b is the species involved in the photosensitization of TiO_2 to visible light. What is not clear from EPR is whether the N-dopant takes substitutional or interstitial positions. A comparison of measured and computed hyperfine coupling constants, Table 1, shows a higher similarity of the experimental parameters for the case of N_i. However, a conclusive assignment needs further additional evidence.

This comes from an ad-hoc experiment consisting of the addition of N atoms to the TiO_2 matrix, thus overcoming the inherent complexity of wet chemical processes that can result in multiple doping species. A thermally reduced sample of polycrystalline TiO_2 was exposed to N atoms generated in a molecular nitrogen plasma.[19] The atoms diffuse into the TiO_2 lattice and more likely occupy the interstitial sites. In order to establish the chemical nature of the formed N species, XPS measurements were coupled to EPR experiments. In fact, N_i and N_s species are expected to give rise to different XPS peaks, due to the different chemical environment: low binding energy (BE) peaks around 396 eV are assigned to N_s atoms, while high BE XPS signals, around 400 eV, are usually associated with N_i species.[19] The appearance of a distinct XPS peak at 400.8 eV for the N–TiO_2 prepared via sol–gel allowed the identification of the N-species as interstitial nitrogen and corroborates the tentative assignment done based on the comparison of measured and computed hfcc's, Table 1. Notice, however, that the nature of the defects introduced in the material strongly depends on the synthetic method used.

2.3. N-Doping of ZnO

The incorporation of N atoms in the ZnO lattice has been proposed as an effective way to achieve p-type doping of this material, which is fundamental for optoelectronic[21] as well as photochemical applications.[22] N atoms can be incorporated in the host ZnO crystal by annealing polycrystalline ZnO in an NH_3 atmosphere.[23] A monomeric paramagnetic species has been identified by low-temperature EPR experiments ($T < 6$ K). The species is photoactive, and the EPR spectral intensity increases under irradiation with visible light. The spin Hamiltonian parameters for this species clearly indicate that the unpaired electron is localized in the N 2p orbitals. The species can thus be described in terms of a N_b dopant with electronic configuration $2s^2p^5$ and formal charge −2 as in the case of N–TiO_2.

Several possible modes of insertion of N in the bulk of ZnO exist, but we concentrate on substitutional to O and interstitial dopants, Figure 1.[23] For N_s species, there is only a very tiny structural rearrangement after doping, and the corresponding impurity states are only 0.30 eV above the top of the VB. The spin density plot looks like a N 2p function, Figure 1.

N can enter the ZnO lattice interstitial sites in two ways, occupying either the octahedral ($N_{i\text{-}Oct}$) or the tetrahedral ($N_{i\text{-}Tet}$) voids. Energy considerations are in favor of the octahedral site, but the two interstitials present very similar electronic features. In the octahedral site, N is inserted between

Table 1. Computed and Measured Hyperfine Coupling Constants (in G) for N-Doped TiO_2 (anatase), ZnO, and MgO Samples

	N_s (substitutional)				N_i (interstitial)				expt			
oxide	a_{iso}	B_1	B_2	B_3	a_{iso}	B_1	B_2	B_3	a_{iso}	B_1	B_2	B_3
TiO_2[20]	14.5	−12.0	−11.7	23.7	11.8	−11.6	−10.0	21.6	13.0	−10.0	−10.0	20.0
ZnO[23]	7.0	−11.1	−11.1	22.1	11.0	−13.5	−12.7	26.2	7.6	−10.7	−10.7	21.4
MgO[29]	13.6	−11.9	−11.9	23.8	13.0	−11.8	−11.3	23.2				

dx.doi.org/10.1021/ar4002944 | Acc. Chem. Res. 2014, 47, 3233–3241

a lattice O and two adjacent Zn ions, resulting in a twisted $(Zn)_2N-O(Zn)_2$ fragment, Figure 1. The N−O distance is 1.38 Å. Two π^*-type spin up α states are at 0.52 and 0.97 eV above the VB, Figure 1. The spin density plot indicates an asymmetric distribution (0.88e on N and 0.12e on O, according to a Mulliken spin population analysis). This is very similar to the electronic structure of N_i in TiO_2.

The comparison of experimental and computed hfcc's allows a clear assignment of the experimental features.[23] In fact, the computed hfcc's of the N_s species fit extremely well with the experimental data, Table 1. For the interstitial species, the agreement is poorer both for the a_{iso} and for the dipolar part. The preference for substitutional N doping is also in line with a thermodynamic analysis of stability.[23] Thus, while in the TiO_2 sample the paramagnetic N-dopant is interstitial, in ZnO the same defect is substitutional.

2.4. N-Doped MgO

The possibility to introduce magnetic defects in wide gap semiconductors or in insulators has attracted considerable interest in recent years.[24] Ferromagnetism in doped insulating oxides is of great importance in the field of spintronics, and diluted magnetic semiconductors are considered to be fundamental materials in this field. Attempts have been made to obtain useful ferromagnetic order in oxide materials by doping with transition metal (TM) or rare earth atoms.[25] However, due to the intrinsic magnetic behavior of TMs, the induced magnetic properties of the doped material are often difficult to discriminate from those of other magnetic impurities.[25] A few attempts to prepare N-doped MgO have been successful, in particular based on molecular beam epitaxy[26,27] or oxidation of metal nitrides.[28] In this latter study, N-doped MgO samples have been prepared by direct oxidation of Mg_3N_2 at high temperature.[28] The oxidized sample contains paramagnetic N centers, and the EPR spectrum displays a pattern typical of one electron interacting with two equivalent nuclei of spin one. Direct comparison with DFT calculations has led to the unambiguous identification of the paramagnetic center as a N_2^- radical anion trapped in the MgO matrix.[28] So far, no other EPR data exist on N-doped MgO, so there are no data available to characterize the single N-impurity species.

The calculations show that when a lattice O^{2-} ion of MgO is replaced by N, one forms a N_s radical species with formal charge −2 (Mulliken charge −2.2). The unpaired electron resides in a 2p orbital, and the spin population on N, 0.86e, suggests strong localization on the impurity atom.[29] The corresponding band has no dispersion (bandwidth of ∼0.1 eV). The three occupied levels are 0.5 eV above the VB, Figure 1.

In Table 1 are reported the hfcc's of the unpaired electron with the ^{14}N nucleus. As we mentioned above, no comparison with experiment is possible. The a_{iso} of N_s is 13.6 G, while the dipolar term is dominant, as expected for an unpaired electron in a 2p type orbital. The absence of superhyperfine interaction confirms that the spin is rather localized.

Next we consider a N atom in an interstitial position, N_i. The final structure shows the formation of a direct N−O bond and the appearance of a NO unit (N−O distance 1.35 Å), which takes the position of the O^{2-} ion in the lattice. The NO unit is oriented along the diagonal of the cube, Figure 1, and the unpaired electron occupies an orbital with π character. The spin population for this π orbital is 0.73e.

The nature of the electronic states is reminiscent of what is found for N-doped TiO_2 and ZnO. The occupied NO π^*-like states are about 1.4 eV above the top of the VB (Figure 1). With respect to N_s, the states are higher in the gap. As for N_s, no band dispersion is observed for N_i, a sign of a strong localization. The structure of the hfcc's is practically the same as for the N_s center, Table 1. Even if EPR data would be available, a distinction of the two defects based on this comparison would not be possible.

3. ELECTRONIC TRANSITIONS IN OXYGEN DEFICIENT SEMICONDUCTING OXIDES

3.1. Transition Energy Levels

Transition energy levels are a well-established, useful, and relatively cheap (in terms of computational cost) tool to estimate excitation and emission energies in defective semiconductors.[30,31] They allow one to more accurately locate the position of the electronic levels associated with the defects in the band gap of the material, compared with the rather crude approach of using one-electron Kohn−Sham eigenvalues. The definition of transition energy level (ε) is "the Fermi level at which two different charge states (q and $q' = q + 1e^-$) of a defect (D) have the same energy". To determine the value of $\varepsilon(q/q')$, one should start from the formation energies of the defect D in the charge state q, $E_D^{form}(q)$, and q', $E_D^{form}(q')$, defined with respect to energy of the bulk host, E_H, the chemical potential of the species involved in creating the defect, and the Fermi level, E_F.

$$E_D^{form}(q \text{ or } q')(\mu, E_F) = E_{D,q\text{or}q'} - E_H + \sum n_i\mu_i + (q \text{ or } q')[E_v + E_F] \quad (1)$$

However, since $E_D^{form}(q)$ and $E_D^{form}(q')$ are equal when $E_F = \varepsilon(q/q')$, some cancellation effects take place, which lead to the following simple expression for transition energy level:

$$\varepsilon(q/q') = \frac{E_{D,q'} - E_{D,q}}{q - q'} - E_v \quad (2)$$

If the top of the VB (E_v) is set as the zero reference for the Fermi level, the transition energy level for an electronic transition involving one charge is simply the difference between the total energy of the defective model in the charge state q' ($E_{D,q'}$) and that of the defective model in charge state q ($E_{D,q}$). We have further simplified this formula[32] by referring to the Janak's theorem according to which total energy differences between two charge states can be derived from Kohn−Sham (KS) eigenvalues as

$$E_{D,q'} - E_{D,q} = \frac{e_{h+1}(N) + e_{h+1}(N+1)}{2} \quad (3)$$

where $e_{h+1}(N)$ is the KS eigenvalue of the LUMO for the q charge state defect and $e_{h+1}(N+1)$ is the KS eigenvalue of the HOMO for the q' charge state defect. Thus, transition energy levels can be directly derived from KS eigenvalues obtained from standard ground state calculations. Charged calculations are performed in a compensating background of charge.

With this approach[32] optical transition levels, $\varepsilon^{opt}(q/q')$, can be computed at fixed atomic positions (vertical transitions). Ionic relaxation can be taken into account to compute thermodynamic or adiabatic transition energy levels, $\varepsilon^{therm}(q/q')$, according to the following equation:

$$\varepsilon^{\mathrm{therm}}(q/q') = \varepsilon^{\mathrm{opt}}(q/q') \pm E_{\mathrm{rel}} \quad (4)$$

where E_{rel} is the relaxation energy in absolute value, as computed from total energies difference between the charged state q' and q in their respective relaxed configuration.

Optical and thermodynamic transition levels are then inserted between the top of the valence band (VB) and the bottom of the conduction band (CB) as in Figure 2. The

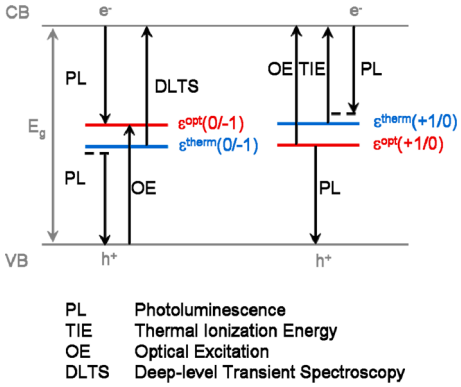

Figure 2. Schematic representation of electronic transitions in defective semiconductors in relation to the spectroscopic techniques that can probe them. The ↑ arrows indicate an electron excitation; the ↓ arrows indicate an electron decay. $\varepsilon^{\mathrm{therm}}$ and $\varepsilon^{\mathrm{opt}}$ are defined with respect to the VB maximum for (0,−1) and (+1,0) charge state transitions.

accuracy of this procedure[32] is related to the fact that the experimental band gap value is rather accurately reproduced by the Kohn−Sham gap obtained with the hybrid functional used. The real meaning of transition energy levels is made explicit in Figure 2 by considering the experimental spectroscopic techniques producing a comparable observable. We have schematically represented how the transition energy levels for (0/−1) and (+1/0) transitions can be related to experimental data. For a more detailed analysis and discussion, see ref 32.

In the following we will analyze optical and thermodynamic transition levels for oxygen deficient semiconducting oxides. In particular, we will focus attention on the oxygen vacancy (V_O) defect in bulk rutile TiO_2, wurzite ZnO, and room-temperature (RT) monoclinic WO_3, trying to compare computed excitation and emission energies with available experimental measurements.

3.2. TiO_{2-x}

The oxygen deficiency in rutile TiO_2 is often observed[33] as a consequence of the sample thermal treatment and is confirmed by some experimental fingerprints such as the intrinsic blue color, the presence of a feature at about 1 eV below the bottom of the CB in the ultraviolet photoelectron (UPS)[34] and electron energy loss (EELS)[35] spectra, and finally a shift of the core level binding energies[36] for the titanium ion associated with a reduction from Ti^{4+} to Ti^{3+}, following the formation of O vacancies or Ti interstitials. EPR has also been recently used to prove the existence of self-trapped electrons at Ti^{3+} centers in bulk rutile powders[37] and single crystals.[38] Hybrid density functional methods (e.g., B3LYP) correctly reproduce, for a model of neutral oxygen vacancy (V_O^0, costing 5.4 eV with respect to 1/2 O_2), the presence of localized defect states detached from the bottom of the CB, in contrast with standard semilocal functionals whose intrinsic self-interaction error causes a spurious delocalization of the excess electrons in a state that is highly resonant with the CB.[39] This was found to be the case for the rutile (110) surface and is confirmed here also for the bulk system. In the 72-atom model we used,[40] the spin-polarized solution with two parallel spins for the excess electrons (triplet state, which was reported in ref 41 to be nearly degenerate to the open shell ground state singlet) is 1.05 eV more stable than the spin-paired (close-shell singlet) solution. Most of the associated spin density is found to be localized on the two under-coordinated Ti ions (at a distance of 3.14 Å) with a consistent contribution also from a third, fully coordinated Ti ion in the same row (see Figure 3). The relaxed singly charged oxygen vacancy model (V_O^+) unexpectedly presents the unpaired electron as mainly localized on this 6-fold Ti ion (0.70), with only some contribution from the two undercoordinated Ti ions (0.15e each at a distance of 3.25 Å). Thus, we can say that most of the excess electron has left the vacancy site and has been trapped by a fully coordinated Ti ion in the neighborhood. It is important to mention that the unpaired electron localization is dependent on the V_O concentration.[41] Note that larger and more realistic supercell models have been considered in refs 41 and 43. Finally, in the relaxed doubly charged oxygen vacancy model (V_O^{2+}), the Ti_{5c}−Ti_{5c} distance is about the same as that in V_O^+ (3.30 Å).

The blue color observed for the reduced rutile TiO_2 samples can be rationalized in terms of d−d transitions (from t_{2g} to e_g states). The vertical excitation of electrons from the defect states to the CB minimum corresponds to the quantity $E_g - \varepsilon^{\mathrm{opt}}$, which is 0.57 eV for the first excitation, 0.85 eV for the second excitation, and 0.71 eV for the double excitation. These values are consistent with the observed features in the UPS and EELS spectra, about 1 eV below the bottom of the CB. However, since the Ti 3d e_g states are not in the bottom part of the CB, the energy associated with the d−d transitions, observed in the optical spectra, will be higher than $E_g - \varepsilon^{\mathrm{opt}}$ and thus in the visible region.

The thermodynamic transition levels are significantly higher in energy than the optical ones. In the case of a (+1/0) transition, the level is found to be above the bottom of the CB, indicating a very easy thermal ionizability of this donor level. These thermal excitations, corresponding quantitatively to $E_g - \varepsilon^{\mathrm{therm}}$, can be compared with experimentaly reported measurements between 0.3 and 0.6 eV from the thermoluminescence (TL) and thermally stimulated current experiments (TSC).[42] While, as we just mentioned, there is virtually no excitation energy in the case of the first (0,+1) excitation, for the second one (+1,+2), we compute an excitation energy of 0.46 eV, in excellent agreement with experiments.

The optical and thermodynamic transition levels reported in the present study are very similar to those reported in previous work based on the GGA+U approach,[43] while they are shallower than those reported in a recent study based on the HSE functional.[41] As already pointed out,[43] the general picture that can be drawn from the computed optical vs thermodynamic transition levels, independently of the specific values obtained, can nicely reconcile why defective rutile TiO_2 systems are spectroscopically identified to present deep donor levels (see optical or vertical excitations) but contextually recognized as n-type conductors (see thermal or adiabatic excitations).

3.3. ZnO_{1-x}

The oxygen vacancy is probably the most studied and the most controversial native defect in ZnO.[44−46] For a long time, it has

dx.doi.org/10.1021/ar4002944 | Acc. Chem. Res. 2014, 47, 3233−3241

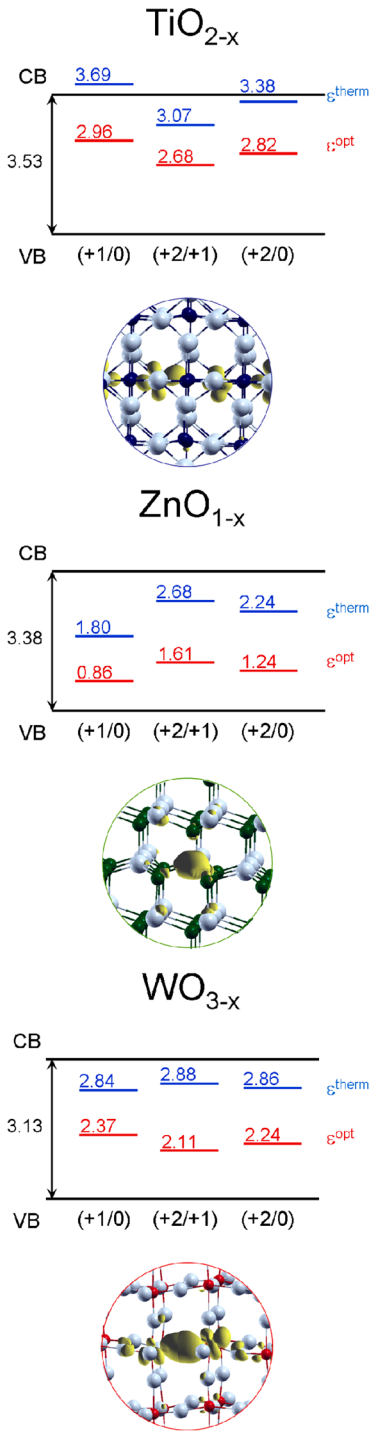

Figure 3. Schematic representation of optical (red) and thermodynamic (blue) transition levels in the band gap of the material (top) and ball-and-stick representation with spin or electron density plot (yellow) for the V_O defect (bottom) for rutile TiO_2, wurzite ZnO, and RT monoclinic WO_3. Ti atoms in blue, Zn atoms in green, W atoms in red, and O atoms in gray.

been considered responsible for shallow donor species causing the unintentional n-type conductivity in the material. The paramagnetic V_O^+ species, created by high energy irradiation of a single crystal, was found to give rise to an EPR signal with axial **g**-tensor of $g_{\parallel} = 1.9948$ and $g_{\perp} = 1.9963$.[47] Quantum mechanical calculations[46,48,49] have shown that O vacancies create well localized electronic levels in the band gap and behave like a deep donor with negative **U** character so that the V_O^+ species is thermodynamically unstable and can only be observed under irradiation. Thus, it is clear now that V_O cannot be responsible for the unintentional n-type conductivity of ZnO.

Hybrid functional B3LYP calculations show that the presence of a neutral V_O center induces a moderate lattice relaxation with an inward displacement of the four nearest Zn ions.[32] The spin-paired configuration of the two excess electrons deriving from the removal of an oxygen atom in a 108-atom supercell model is more stable than the spin-parallel one by 2.9 eV. The two electrons are localized in a flat electronic state, which is 0.6 eV above the top of the VB. The electron density plot clearly shows that this defect state is highly localized in the vacancy but has also some contribution from the undercoordinated Zn ions (see Figure 3). The ionization of V_O to form V_O^+ and V_O^{2+} causes a large outward relaxation of the zinc ions. The large lattice relaxation for the double charged vacancy significantly reduces its formation energy,[48] favoring the negative-**U** character of V_O. In fact, on the basis of the computed thermodynamic transition levels, $\varepsilon^{therm}(+1/0) = 1.81$ eV and $\varepsilon^{therm}(+2/+1) = 2.69$ eV, we find that the V_O^+ state is always thermodynamically unstable for any value of the Fermi level. Below a Fermi level of 1.8 eV the most stable species is V_O^{2+}; above a Fermi level of 2.7 eV, the most stable species is V_O^0. The transition level, $\varepsilon^{therm}(+2/0)$, is computed to be 2.24 eV (see Figure 3), in excellent agreement with the values obtained by plane-wave calculations[46,48] in the range of 1.9−2.4 eV.

Contrasting data are present in the literature as regards the V_O formation energy, which was computed to be either very high ($\Delta H \approx 4$ eV) in O-poor/Zn-rich conditions[44,49] or very low ($\Delta H \approx 1$ eV).[48,50] We have determined[32] a formation energy of 3.5 eV for V_O in ZnO with respect to 1/2 O_2. Going to oxygen poor conditions, the formation energy decreases considerably.

Finally, the green luminescence of ZnO (~2.45 eV) has been reported as evidence of the presence of V_O in bulk ZnO. We estimated the excitation energy (exp. 3.1 eV) as the energy associated with the process: $V_O \rightarrow V_O^+ + e^-_{CB}$, which is $E_g - \varepsilon^{opt}(+1/0) = 2.53$ eV. The emission can be the consequence of the recombination of either (i) the excited electron with the hole at the defect level, for (+1/0) = 0.80 eV and for (+2/+1) = 0.20 eV, or (ii) the electron in the defect state with the hole at the top of the VB, $\varepsilon^{opt}(+1/0) = 0.86$ eV, $\varepsilon^{opt}(+2/+1) = 1.61$ eV, and $\varepsilon^{opt}(+2/0) = 1.24$ eV. We tentatively assign the observed photoluminescence (~2.45 eV) to the $V_O^+ \rightarrow V_O^{2+} + e^-_{VB}$ transition (i.e., $\varepsilon^{opt}(+2/+1) = 1.61$ eV), which presents the closest emission energy, in line with previous work.[44]

3.4. WO_{3-x}

The removal of one oxygen atom in a 64-atom supercell model of RT monoclinic WO_3 costs about 5.3 eV with respect to 1/2 O_2 according to B3LYP calculations.[51] The spin-paired (singlet) configuration is 0.21 eV more stable then the spin-parallel (triplet). The electron density plot (Figure 3) indicates that most of the excess electrons are localized at the V_O site, although, similarly to the ZnO case, tails of the density are also on the 5d orbitals of the two undercoordinated W ions pointing toward the defect void. Thus, one can simplify this situation with the following synthetic expression: $W^{6+}/V_O(2e^-)/W^{6+}$, which indicates that the oxidation state of the undercoordinated W ions is still formally +6 while the two extra electrons are trapped in the vacancy void.

dx.doi.org/10.1021/ar4002944 | Acc. Chem. Res. 2014, 47, 3233−3241

The commonly observed blue coloration of WO_{3-x} is a consequence of light absorption in the visible,[52] and oxygen vacancies are suggested to be the species at the origin of this optical transition.[3] We have computed the B3LYP optical transition levels, ε^{opt}, for the (+1/0), (+2/+1), and (+2/0) charge transitions involving the V_O defect states. They are located at 2.37, 2.11, and 2.24 eV, respectively, above the top of VB (see Figure 3), with a band gap value of 3.13 eV in good agreement with recent more refined calculations.[53] Thus, the electronic vertical transitions to the bottom of the CB ($E_g - \varepsilon^{opt}$) have energies of about 1 eV. Since the electronic transitions involve states above the CB minimum ($t_{2g} \rightarrow e_g$),[54] analogously to TiO_2 (see above), they will fall in the visible region and can account for the blue coloration of WO_{3-x}. The optical transition levels are also consistent with the photoluminescence (PL) emission peak at about 550 nm (~2.26 eV), which was attributed to oxygen vacancies,[55] with photoelectron[56,57] and electron energy loss[58] measurements on nonstoichiometric films and single crystals.

It is very important to stress that the *semiconducting* character of the band structure of WO_{3-x} with $x = 0.0625$, found with the hybrid functional B3LYP, is in net contrast with previous studies based on standard LDA or GGA methods[59,60] where the defect state is resonant with the bottom of the CB.

To conclude, we comment on how the computed electronic transitions involving different V_O charge states (from 0 to 2+) in WO_{3-x} compare with the Deb's proposed model for the electrochromic effect observed for oxygen deficient WO_3.[3] According to this model, the V_O^0 defect state lies within the VB, while the V_O^+ is in the band gap and the V_O^{2+} is inside the CB. This fits quite nicely with the B3LYP Kohn–Sham levels in the gap, except for the neutral defect V_O^0, which we find to be in the middle of the band gap. In general, the idea of Deb's model that different charge states of the defect give rise to different transitions is in line with our results. Neutral and singly charged defects cause transitions in the visible region [(0/+1), (+1/+2), and (0/+2)] (colored oxide). If the doubly charged state is reached, all optical absorption properties of the material are quenched since no more defect states are present in the band gap (transparent oxide). This model can nicely explain the electrochromic effect, that is, the reversible change in color (colored ↔ transparent) observed for this material when a voltage is applied.

4. SUMMARY AND OUTLOOK

In the first part of this Account (section 2), we have seen that the nature of nitrogen substitutional or interstitial impurities is very similar in three oxides with quite different electronic and geometric structure. This is due to the local nature of the unpaired electron characterizing these defects. The comparison of computed and measured hfcc's provides a powerful tool to determine the level of spin localization. The electron localization has the consequence that the corresponding impurity states in the band gap of the material are also localized and do not form wide bands. This is detrimental for the photocatalytic activity since localized holes act as recombination centers and lower the efficiency of the photocatalyst. This is clearly shown by calculations including in the same model both an N-dopant (either N_s or N_i) and Ti^{3+} center. The Ti^{3+} $3d^1$ state is close to the CB, that is, much higher in energy that the N 2p states. A spontaneous electron transfer occurs from these high lying states and N, according to the reaction: $N_b^{\bullet} + Ti^{3+\bullet}$ (triplet state) → $N_b^- + Ti^{4+}$ (singlet state), Figure 4. Electrons promoted by light into the CB when in the proximity of a N-defect will be trapped reducing the

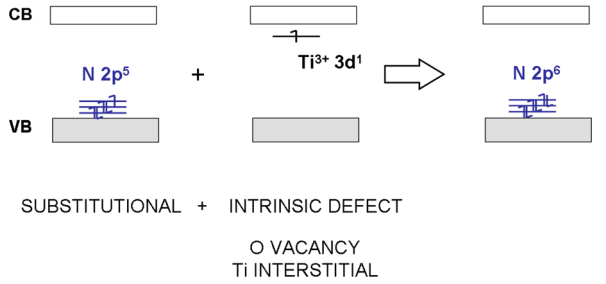

Figure 4. Schematic representation of electron transfers between one-electron levels of substitutionally N-doped and reduced anatase TiO_2.

number of carriers. Similar processes occur for N–ZnO and N–MgO and are related to the presence of low-lying acceptor states in the band gap. A proper and complete characterization of the defect electronic structure is therefore of fundamental importance for the design of new photoactive materials.

In the second part of this Account (section 3), we have shown how it is possible to compute optical and thermodynamic transition levels for defect centers in semiconducting oxides and directly compare them to available experimental data. The oxygen deficient semiconducting oxides TiO_2 (rutile), ZnO (wurzite), and WO_3 (RT monoclinic structure) have been taken as explicative examples. The nature of V_O was found to be rather different in the three cases. While for rutile TiO_2 the removal of one neutral oxygen atom leads to the reduction of Ti^{4+} to Ti^{3+} ions, in the case of ZnO and WO_3 the excess electron density is found to be localized at the vacancy site, in analogy with what typically happens in insulating oxides: the so-called F centers. The optical transition levels (vertical excitations) for the V_O defect are progressively less deep going from ZnO to WO_3 to TiO_2, although in all three cases this type of defect should be considered as a deep donor. The thermodynamic transition levels (adiabatic excitations) are still quite deep for ZnO and WO_3, while in the case of TiO_2 they are very close to, if not resonant with, the bottom of the CB, confirming the n-type conductivity of oxygen deficient TiO_2. The comparative analysis has revealed a closer similarity between ZnO_{1-x} and WO_{3-x} systems with respect to TiO_{2-x} in terms of both the chemical and physical nature of the defect and the electronic structure modifications deriving from its presence.

■ AUTHOR INFORMATION

Corresponding Authors

*E-mail: cristiana.divalentin@mater.unimib.it.
*E-mail: gianfranco.pacchioni@mater.unimib.it.

Notes

The authors declare no competing financial interest.

Biographies

Cristiana Di Valentin was born in Maniago (PN) on 29/07/1973. She graduated in Chemistry in 1997 at the University of Pavia where she also received her Ph.D. degree in 2000 in collaboration with the Technische Universität München. She was appointed by the University of Milano Bicocca as Assistant Professor in 2002 and as Associate Professor of General and Inorganic Chemistry in 2012. She has been visiting scientist at Princeton University, Universitat de

Barcelona, and Ecole Nationale Superieure de Paris. Her research interests span from ab initio computational study of reaction mechanisms in organic chemistry and homogeneous catalysis to heterogeneous catalysis, photocatalysis, doped and defective semiconducting oxides, graphene, and carbon based materials for fuel cells.

Gianfranco Pacchioni was born in Milano on 08/11/1954. He received his Ph.D. at the Freie Universität Berlin in 1984. He worked at the IBM Almaden Research Center and the Technical University of Munich. He is Full Professor of Solid State Chemistry at the University of Milano Bicocca and has been Director of the Department of Materials Science from 2003 to 2009. He received various awards including the Humboldt Award (2005). He is presently Vice Rector for Research of the University Milano Bicocca and member of the scientific council of various journals, foundations, and consortia. He has published more than 400 papers on the electronic structure of oxide surfaces and interfaces, supported metal clusters, and their role in catalysis.

■ ACKNOWLEDGMENTS

We thank our former collaborators F. Gallino and F. Wang for their valuable contribution to this work. We acknowledge the financial support by MIUR (FIRB-RBAP11AYN) and by the COST Action CM1104. We thank Regione Lombardia for the computational resources through a LISA Initiative at CINECA (LI01p_VISFOTOCAT).

■ REFERENCES

(1) Asahi, R.; Morikawa, T.; Ohwaki, T.; Aoki, K.; Taga, Y. Visible-Light Photocatalysis in Nitrogen-Doped Titanium Oxides. *Science* **2001**, *293*, 269−271.
(2) Minami, T.; Nanto, H.; Takata, S. Highly Conductive and Transparent Zinc Oxide Films Prepared by rf Magnetron Sputtering under an Applied External Magnetic Field. *Appl. Phys. Lett.* **1982**, *41*, 958−960.
(3) Deb, S. K. Opportunities and Challenges in Science and Technology of WO_3 for Electrochromic and Related Applications. *Sol. Energy Mater. Sol. Cells* **2008**, *92*, 245−258.
(4) McFarland, E. W.; Metiu, H. Catalysis by Doped Oxides. *Chem. Rev.* **2013**, *113*, 4391−4427.
(5) Ganduglia-Pirovano, M. V.; Hofmann, A.; Sauer, J. Oxygen Vacancies in Transition Metal and Rare Earth Oxides: Current State of Understanding and Remaining Challenges. *Surf. Sci. Rep.* **2007**, *62*, 219−270.
(6) Pascual, J.; Camassel, J.; Mathieu, H. Fine Structure in the Intrinsic Absorption Edge of TiO_2. *Phys. Rev. B* **1978**, *18*, 5606−5614.
(7) Tang, H.; Lévy, F.; Berger, H.; Schmid, P. E. Urbach Tail of Anatase TiO_2. *Phys. Rev. B* **1995**, *52*, 7771−7774.
(8) Reynolds, D. C.; Look, D. C.; Jogai, B.; Litton, C. W.; Cantwell, G.; Harsch, W. C. Valence-Band Ordering in ZnO. *Phys. Rev. B* **1999**, *60*, 2340−2344.
(9) Johansson, M. B.; Baldissera, G.; Valyukh, I.; Persson, C.; Arwin, H.; Niklasson, G. A.; Österlund, L. Electronic and Optical Properties of Nanocrystalline WO_3 Thin Films Studied by Optical Spectroscopy and Density Functional Calculations. *J. Phys.: Condens. Matter* **2013**, *25*, No. 205502.
(10) Whited, R. C.; Flaten, C. J.; Walker, W. C. Exciton Thermoreflectance of MgO and CaO. *Solid State Commun.* **1973**, *13*, 1903−1905.
(11) Muscat, J.; A; Wander, A.; Harrison, N. M. On the Prediction of Band Gaps from Hybrid Functional Theory. *Chem. Phys. Lett.* **2001**, *342*, 397−401.
(12) Becke, A. D. Density-Functional Thermochemistry. III. The Role of Exact Exchange. *J. Chem. Phys.* **1993**, *98*, 5648−5652. Lee, C.; Yang, W.; Parr, R. G. Development of the Colle-Salvetti Correlation-Energy Formula into a Functional of the Electron Density. *Phys. Rev. B* **1988**, *37*, 785−789.
(13) Heyd, J.; Scuseria, G. E.; Ernzerhof, M. Hybrid Functionals Based on a Screened Coulomb Potential. *J. Chem. Phys.* **2006**, *124*, No. 219906.
(14) Dovesi, R.; Saunders, V. R.; Roetti, C.; Orlando, R.; Zicovich-Wilson, C. M.; Pascale, F.; Civalleri, B.; Doll, K.; Harrison, N. M.; Bush, I. J.; D'Arco, P.; Llunell, M.; *CRYSTAL09 User's Manual*; University of Torino: Torino, Italy, 2009.
(15) Weil, J. A.; Bolton, J. R.; Wertz, J. E. *Electron Paramagnetic Resonance*; John Wiley & Sons: New York, 1994.
(16) Chiesa, M.; Giamello, E.; Che, M. EPR Characterization and Reactivity of Surface-Localized Inorganic Radicals and Radical Ions. *Chem. Rev.* **2010**, *110*, 1320−1347.
(17) Fujishima, A.; Zhang, X.; Tryk, D. A. TiO_2 Photocatalysis and Related Surface Phenomena. *Surf. Sci. Rep.* **2008**, *63*, 515−582.
(18) Henderson, M. A. A Surface Science Prospective on TiO_2 Photocatalysis. *Surf. Sci. Rep.* **2011**, *66*, 185−297.
(19) Napoli, F.; Chiesa, M.; Livraghi, S.; Giamello, E.; Agnoli, S.; Granozzi, G.; Pacchioni, G.; Di Valentin, C. The Nitrogen Photoactive Centre in N-Doped Titanium Dioxide Formed via Interaction of N Atoms with the Solid. Nature and Energy Level of the Species. *Chem. Phys. Lett.* **2009**, *477*, 135−138.
(20) Di Valentin, C.; Finazzi, E.; Pacchioni, G.; Selloni, A.; Livraghi, S.; Paganini, M. C.; Giamello, E. N-Doped TiO_2: Theory and Experiment. *Chem. Phys.* **2007**, *339*, 44−56.
(21) Liu, L.; Xu, J.; Wang, D.; Jiang, M.; Wang, S.; Li, B.; Zhang, Z.; Zhao, D.; Shan, C.-X.; Yao, B.; Shen, D. Z. p-Type Conductivity in N-Doped ZnO: The Role of the N_{Zn}-V_O Complex. *Phys. Rev. Lett.* **2012**, *108*, No. 215501.
(22) Yang, X.; Wolcott, A.; Wang, G.; Sobo, A.; Fitzmorris, R. C.; Qian, F.; Zhang, J. Z.; Li, Y. Nitrogen-Doped ZnO Nanowire Arrays for Photoelectrochemical Water Splitting. *Nano Lett.* **2009**, *9*, 2331−2336.
(23) Gallino, F.; Di Valentin, C.; Pacchioni, G.; Chiesa, M.; Giamello, E. Nitrogen Doped Polycrystalline ZnO. A Combined Pulse EPR and DFT Study. *J. Mater. Chem.* **2010**, *20*, 689−697.
(24) Dietl, T. A Ten-Year Perspective on Dilute Magnetic Semiconductors and Oxides. *Nat. Mater.* **2010**, *9*, 965−974.
(25) Ogale, S. B. Dilute Doping, Defects, and Ferromagnetism in Metal Oxide Systems. *Adv. Mater.* **2010**, *22*, 3125−3155.
(26) Grob, M.; Pratzer, M.; Morgentstern, M.; Lezaic, M. Catalytic Growth of N-doped MgO on Mo(001). *Phys. Rev. B* **2012**, *86*, No. 075455.
(27) Jiang, X.; Parkin S. S. P.; Samant M. G.; Yang, C.-H.; Resistive switching in Nitrogen-doped MgO. US Patent 8,227,896, B2, 2012.
(28) Napoli, F.; Chiesa, M.; Giamello, E.; Fittipaldi, M.; Di Valentin, C.; Gallino, F.; Pacchioni, G. N_2^- Radical Anions Trapped in Bulk Polycrystalline MgO. *J. Phys. Chem. C* **2010**, *114*, 5187−5192.
(29) Pesci, M.; Gallino, F.; Di Valentin, C.; Pacchioni, G. Nature of Defect States in Nitrogen-Doped MgO. *J. Phys. Chem. C* **2010**, *114*, 1350−1356.
(30) Lany, S.; Zunger, A. Assessment of Correction Methods for the Band-Gap Problem and for Finite-Size Effects in Supercell Defect Calculations: Case Studies for ZnO and GaAs. *Phys. Rev. B* **2008**, *78*, No. 235104.
(31) Van de Walle, C. G.; Neugebauer, J. First-Principles Calculations for Defects and Impurities: Applications to III-Nitrides. *J. Appl. Phys.* **2004**, *95*, 3851−3879.
(32) Gallino, F.; Pacchioni, G.; Di Valentin, C. Transition Levels of Defect Centers in ZnO by Hybrid Functionals and Localized Basis Set Approach. *J. Chem. Phys.* **2010**, *133*, No. 144512.
(33) Diebold, U. The Surface Science of Titanium Dioxide. *Surf. Sci. Rep.* **2003**, *48*, 53−229.
(34) Nolan, M.; Elliot, S. D.; Mulley, J. S.; Bennet, R. A.; Basham, M.; Mulheran, P. Electronic Structure of Point Defects in Controlled Self-Doping of the TiO_2 (110) Surface: Combined Photoemission Spectroscopy and Density Functional Theory Study. *Phys. Rev. B* **2008**, *77*, No. 235424.

(35) Henderson, M. A.; Epling, W. S.; Peden, C. H. F.; Perkins, C. L. Insights into Photoexcited Electron Scavenging Processes on TiO_2 Obtained from Studies of the Reaction of O_2 with OH Groups Adsorbed at Electronic Defects on TiO_2(110). *J. Phys. Chem. B* **2003**, *107*, 534−545.
(36) Nerlov, J.; Christensen, S. V.; Wichel, S.; Pedersen, E. H.; Møller, P. J. A Photoemission Study of the Coadsorption of CO_2 and Na on TiO_2(110)-(1 × 1) and -(1 × 2) Surfaces: Adsorption Geometry and Reactivity. *Surf. Sci.* **1997**, *371*, 321−336.
(37) Livraghi, S.; Maurelli, S.; Paganini, M. C.; Chiesa, M.; Giamello, E. Probing the Local Environment of Ti^{3+} Ions in TiO_2 (Rutile) by ^{17}O HYSCORE. *Angew. Chem., Int. Ed.* **2011**, *50*, 8038−8040.
(38) Yang, S.; Brant, A. T.; Giles, N. C.; Halliburton, L. E. Intrinsic Small Polarons in Rutile TiO_2. *Phys. Rev. B* **2013**, *87*, No. 125201.
(39) Di Valentin, C.; Pacchioni, G.; Selloni, A. Electronic Structure of Defect States in Hydroxylated and Reduced Rutile TiO_2(110) Surfaces. *Phys. Rev. Lett.* **2006**, *97*, No. 166803.
(40) The calculations were done for bulk rutile 2 × 2 × 3 supercell model (72-atoms) with the B3LYP functional, as implemented in the CRYSTAL09 code, and the all-electron basis sets O 8-411(d1), Ti 86-411(d41). The *k*-space sampling for the bulk geometry optimizations includes eight *k* points.
(41) Deak, P.; Aradi, B.; Frauenheim, T. Quantitative Theory of the Oxygen Vacancy and Carrier Self-Trapping in Bulk TiO_2. *Phys. Rev. B* **2012**, *86*, No. 195206.
(42) Ghosh, A. K.; Wakim, F. G.; Addiss, R. R., Jr. Photoelectronic Processes in Rutile. *Phys. Rev.* **1969**, *184*, 979−988.
(43) Mattioli, G.; Alippi, P.; Filippone, F.; Caminiti, R.; Amore Bonapasta, A. Deep versus Shallow Behavior of Intrinsic Defects in Rutile and Anatase TiO_2 Polymorphs. *J. Phys. Chem. C* **2010**, *114*, 21694−21704.
(44) Janotti, A.; Van de Walle, C. G. Fundamentals of Zinc Oxide As a Semiconductor. *Rep. Prog. Phys.* **2009**, *72*, No. 126501.
(45) McCluskey, M. D.; Jokela, S. J. Defects in ZnO. *J. Appl. Phys.* **2009**, *106*, No. 071101.
(46) Lany, S.; Zunger, A. Assessment of Correction Methods for the Band-Gap Problem and for Finite-Size Effects in Supercell Defect Calculations: Case Studies for ZnO and GaAs. *Phys. Rev. B* **2008**, *78*, No. 235104.
(47) Smith, J. M.; Vehse, W. E. ESR of Electron Irradiated ZnO Confirmation of the F^+ Center. *Phys. Lett. A* **1970**, *31*, 147−148.
(48) Oba, F.; Togo, A.; Tanaka, I.; Paier, J.; Kresse, G. Defect Energetics in ZnO: A Hybrid Hartree-Fock Density Functional Study. *Phys. Rev. B* **2008**, *77*, No. 245202.
(49) Lee, W.-J.; Kang, J.; Chang, K. J. Defect Properties and *p*-type Doping Efficiency in Phosphorus-Doped ZnO. *Phys. Rev. B* **2006**, *73*, No. 024117.
(50) Lany, S.; Zunger, A. Dopability, Intrinsic Conductivity, and Nonstoichiometry of Transparent Conducting Oxides. *Phys. Rev. Lett.* **2007**, *98*, No. 045501.
(51) Wang, F.; Di Valentin, C.; Pacchioni, G. Semiconductor-to-Metal Transition in WO_{3-x}: Nature of Oxygen Vacancy. *Phys. Rev. B* **2011**, *84*, No. 073103.
(52) Rougier, A.; Portemer, F.; Quédé, A.; El Marssi, M. Characterization of Pulsed Laser Deposited WO_3 Thin Films for Electrochromic Devices. *Appl. Surf. Sci.* **1999**, *153*, 1−9.
(53) Ping, Y.; Rocca, D.; Galli, G. Optical Properties of Tungsten Trioxide from First-Principles Calculations. *Phys. Rev. B* **2013**, *87*, No. 165203.
(54) Wang, F.; Di Valentin, C.; Pacchioni, G. Doping of WO_3 for Photocatalytic Water Splitting: Hints from Density Functional Theory. *J. Phys. Chem. C* **2012**, *116*, 8901−8909.
(55) Loopstra, B. O.; Rietvekt, H. N. Further Refinement of the Structure of WO_3. *Acta Crystallogr.* **1969**, *B25*, 1420−1421.
(56) Di Quarto, F.; Di Paola, A.; Sunseri, C. Semiconducting Properties of Anodic WO_3 Amorphous Films. *Electrochim. Acta* **1981**, *26*, 1177−1184.
(57) Hollinger, G.; Duc, T. M.; Deneuville, A. Charge Transfer in Amorphous Colored WO_3 Films Observed by X-Ray Photoelectron Spectroscopy. *Phys. Rev. Lett.* **1976**, *37*, 1564−1567.
(58) Ritsko, J.; Witzke, H.; Deb, S. K. Fast Electron Energy Loss Spectrum of an Amorphous Tungsten Trioxide Film. *Solid State Commun.* **1977**, *22*, 455−458.
(59) Lambert-Mauriat, C.; Oison, V. Density-Functional Study of Oxygen Vacancies in Monoclinic Tungsten Oxide. *J. Phys.: Condens. Matter* **2006**, *18*, 7361−7371.
(60) Chatten, R.; Chadwick, A. V.; Rougier, A.; Lindan, P. J. D. The Oxygen Vacancy in Crystal Phases of WO_3. *J. Phys. Chem. B* **2005**, *109*, 3146−3156.